Synaptic Metaplasticity Realized in Oxide Memristive Devices

Zheng-Hua Tan, Rui Yang, Kazuya Terabe, Xue-Bing Yin, Xiao-Dong Zhang, and Xin Guo**

The human brain is a remarkably powerful yet highly efficient computational device. Within a volume smaller than a shoebox, it performs different cognitive functions of linguistic comprehension, abstract reasoning, and motor control, which are based upon high levels of computation even challenging the largest supercomputer.[1] The high efficiency of the brain is due to its special architecture of operation dominated by synaptic activities, through which information processing and storage occur simultaneously. Biologically, a synapse is formed at the contact junction between two neuron cells in the brain, as shown by **Figure 1**a. When the brain is under an external stimulus, the synapse receives an action potential that induces presynaptic release of neurotransmitter and causes postsynaptic membrane depolarization. This generates across the synapse an excitatory postsynaptic potential (EPSP) or an excitatory postsynaptic current (EPSC), which are used to measure the strength of the synaptic activity, i.e., the "synaptic weight." Furthermore, EPSP or EPSC can be successively modified by the presynaptic action potential in response to external stimuli. This particular feature of the synapse, the so-called "activity-dependent plasticity" in neuroscience, forms a key component of the brain's learning machinery in which the learning activities generate persistent forms of synaptic plasticity for information processing and storage. One type of the activity-dependent plasticity is spike-timing-dependent plasticity (STDP), whose properties depend on the relative timing between the spikes of pre- and postsynaptic action potentials. Specifically, if the presynaptic spike precedes the postsynaptic spike (positive spike-timing interval), long-term potentiation (LTP) is induced; whereas if the presynaptic spike occurs after the postsynaptic spike (negative spike-timing interval), long-term depression (LTD) ensues.[2]

In neuroscience, the conventional approach to study the synapse plasticity is to modulate the plasticity with a potential spike of learning action. In contrast, the metaplasticity approach introduces an episode of priming stimulus at some time before applying the learning action to evoke the synaptic plasticity, such a situation is illustrated in Figure 1b.[3] The key feature of metaplasticity is that a change in the synapse alters its ability for subsequent synaptic plasticity without necessarily affecting the efficacy of normal synaptic transmission.[3] Metaplasticity is a higher-order form of the synaptic plasticity,[4,5] sometimes called the "plasticity of synaptic plasticity," yet it shares with conventional plasticity an extensive range of mechanisms.[3]

Mimicking synaptic plasticity using engineering devices is one of most promising approaches towards the realization of neuromorphic computing, which is one way to overcome the "von Neumann bottleneck" to meet the urgent demand on information processing in the coming Big Data Era. So far, various forms of STDP[6–21] have been demonstrated using memristors[6–20] and the so-called "second-order memristors"[21] in different material systems, including Si:Ag,[6] $Ge_2Sb_2Te_2$,[7,11] nanoparticle/organic,[8] InGaZnO,[9] MgO,[10] TiO_2,[12] AgInSbTe,[13] Ta_2O_5:Si,[14] FeO_x,[15] HfO_2,[16–20] and Ta_2O_5.[21] These studies made great contributions to the development of neuromorphic computing based on memristive devices. However, the metaplasticity has not been taken into consideration in these studies. For an artificial synapse, the activity-dependent plasticity is affected by its sequence of experienced activities as well as rate, interval and amplitude of action potential spikes. The synaptic-weight modulability of an artificial synapse can be significantly different due to different history of spikes applied, clearly demonstrating metaplasticity. Specifically, the interval of the spikes also affects the ability to generate the synaptic plasticity, although there is no agreed criterion for the degree of persistence that is required to meet the definition of metaplasticity.[3] The synaptic weight decay over time is generally observed in biology.[4,5,22,23] The phenomenon of current decaying has also been exhibited in many memristive devices based on various resistive switching mechanisms, e.g., ion migration,[24–26] electron trapping/detraping,[27,28] and phase change.[29–32] The device state varies within a certain time scale, therefore, the spike interval has an important influence on the device state at the time when a following spike is executed, thus further affects the final performance of neuromorphic functions.

In this work, the metaplasticity and STDP are demonstrated in an artificial synapse implemented with a WO_3-based memristive device. In particular, the effect of metaplasticity on the STDP performance of an artificial synapse is systematically investigated through different aspects of activity sequence and spike interval. The artificial synapse in this study shows a bio-realistic behavior, which has great potential for neuromorphic computing applications.

Structures of the WO_3 memristive device before and after the electroforming process were characterized with optical imaging as well as transmission electron microscopy (TEM),

Z.-H. Tan, Dr. R. Yang, X.-B. Yin, Dr. X.-D. Zhang, Prof. X. Guo
Laboratory of Solid State Ionics
School of Materials Science and Engineering
Huazhong University of Science and Technology
Wuhan 430074, P.R. China
E-mail: yangrui@hust.edu.cn; xguo@hust.edu.cn
Dr. K. Terabe
International Center for Materials Nanoarchitectonics (WPI-MANA)
National Institute for Materials Science (NIMS)
1-1 Namiki, Tsukuba, Ibaraki 305-0044, Japan

DOI: 10.1002/adma.201503575

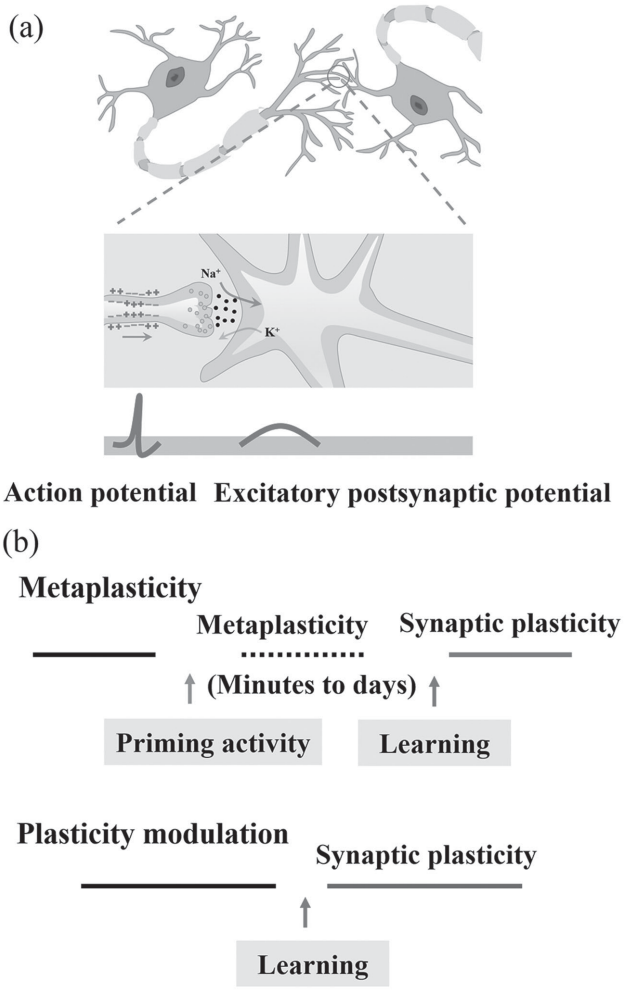

Figure 1. Conceptual schematic of synapse and synaptic plasticity. a) Schematic illustration of a pair of neurons and one synapse between them. The synapse is the connection between the neurons. When an action potential is applied on the presynapse, the excitatory postsynaptic potential (EPSP) is generated in the postsynapse. The synaptic weight can be represented by the relative magnitude of EPSP. b) Standard paradigm for studying metaplasticity. Compared with the conventional modulation of plasticity, a priming activity is applied before evoking synaptic plasticity by another plasticity-inducing event.

and the relevant results are presented in **Figure 2**. The device has a crossbar structure formed with two Pt straps with a thin layer of WO_3 sandwiched in-between (Figure 2a,b). Before electroforming, the WO_3 thin layer was amorphous but dispersed with crystallized nanoparticles with an average diameter of ≈2 nm (Figure 2b,c). After electroforming under current compliance of 1 mA (the inset of Figure 2d), a broken bubble appeared in the lower right corner of the cross point, as highlighted in the square of Figure 2d. It was reported that the resistive switching could be affected by different atmospheres,[33,34] and our previous work demonstrated that oxygen played a key role in the resistive switching of WO_3.[34] Therefore, this bubble is believed to be due to the evolution of oxygen gas from the interface between WO_3 and the Pt top electrode[34,35] in accordance with the reaction of: $O_O^{\times} \leftrightarrow V_O + 2e' + 1/2O_2(\uparrow)$. A similar phenomenon has been previously observed for $SrTiO_3$.[36] A cross-sectional cut was made along the broken bubble using focused ion beam. TEM observations show that WO_3 becomes now crystallized (Figure 2e) with the coexistence of a mother phase as well as a conductive Magnéli phase verified by electron diffraction pattern (Figure 2f). The Magnéli phase should be responsible for the subsequent bipolar resistive switching. This is the first time that the Magnéli phase was directly observed in the WO_3 film after electroforming, although some works assumed that.[34,37]

The conventional synaptic plasticity and metaplasticity are both demonstrated in the WO_3 memristive device as shown by **Figure 3**a. As exhibited in the upper panel, the application of a presynaptic spike (2.1 V, 10 μs) immediately triggers an EPSC with a magnitude of ≈35 nA, which then gradually decays over time and becomes stable in about 1000 s at a level (≈18 nA) higher than the current level before the presynaptic spike application (10 nA). This exactly exhibits the conventional LTP with increased synaptic weight. The state of the memristive device is then reset by applying a negative voltage pulse followed with a one-day relaxation. The metaplasticity was then tested with results given in the lower panel. A priming spike (1.7 V, 10 μs) does not cause any immediate variation in the device current, but allows a 60 nA EPSC to be triggered by the forthcoming presynaptic spike (2.1 V, 10 μs). The EPSC then decays and finally becomes stable at a level of ≈24 nA. Comparing with the conventional LTP in the upper panel, the higher level of EPSC (24 nA vs 18 nA) means a larger change of plasticity for such a synaptic device. In other words, the metaplasticity was realized in this device with its synaptic plasticity modulated by a priming spike. In addition, more detailed information about LTP can be gathered from the decaying curves of both EPSCs. It has been known that the time-dependent LTP in biological systems consists of two periods with different characteristics, namely the early-form LTP and the late-form LTP.[38] The former usually decays over time to some extent whereas the latter keeps stable. The instinctively decaying EPSC realized in the present device clearly mimics the behavior of the biological LTP.

In some cases, the metaplasticity is hardly distinguishable from the conventional plasticity, where the priming spike, which can alter the ability to generate plasticity, changes the synaptic plasticity directly;[3–5] such a case is demonstrated in Figure 3b. Comparing the ESPC in the upper panel with the one in the lower panel, the priming spike (1.8 V, 10 μs) not only allows a higher EPSC to be generated by the presynaptic spike (2 V, 10 μs) but also by itself generates an EPSC and thus changes the plasticity. In this case, the metaplasticity overlaps with the conventional plasticity, which adds considerable complexity for the synaptic plasticity research and might be the reason for pretty few reports on the metaplasticity in artificial synapses.

STDP due to cumulative resistance modulation has also been realized in the WO_3 memristive device. As shown in **Figure 4**a, under stimulation with a sequence of precisely controlled positive and negative pulses, the device exhibits consecutive change of current with decaying properties. In particular, a transition from volatile to nonvolatile resistive switching is achieved as specifically shown in the dotted square. This exactly mimics the transition from the short-term plasticity to the long-term plasticity in biological systems.[39,40] In addition, the conductance

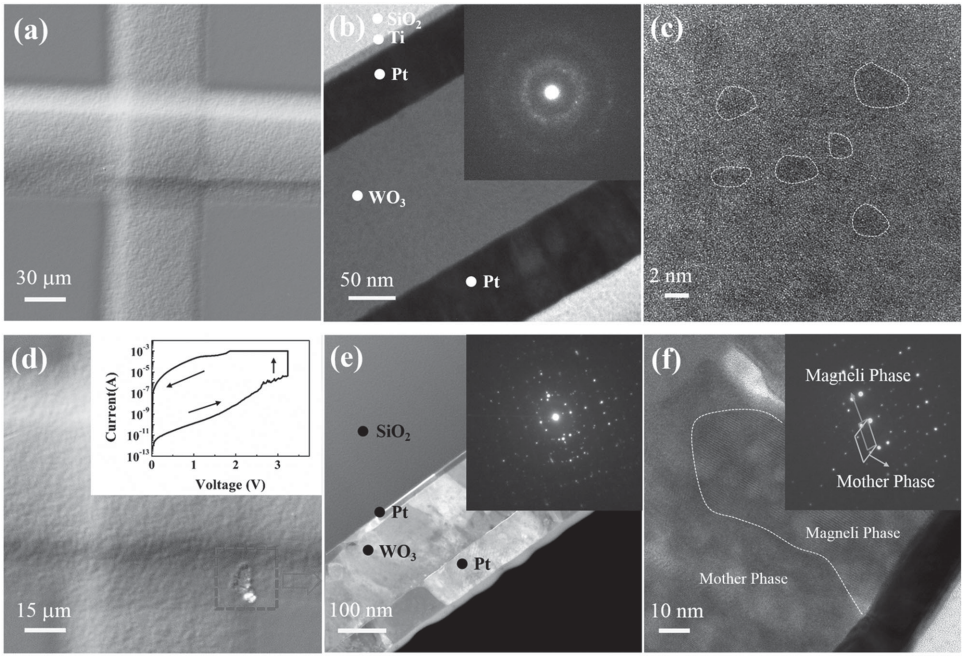

Figure 2. Structural characterization of Pt/WO_3/Pt device. a) Optical image of the crossbar structure. b) TEM image with electron diffraction pattern. c) HRTEM image of WO_3 layer before electroforming. d) Optical image with a bubble in the square and the electroforming curve. e) TEM image of cross-section. f) HRTEM image of WO_3 layer with electron diffraction pattern beneath the bubble after electroforming.

change of the WO_3 device can be used to mimic STDP with precisely engineered pre- and post-spike pulses (the inset in Figure 4b). This overlapping spiking pulse protocol actually builds a connection between Δt and the pulse amplitude, V.[7,10,11,13,14] As illustrated in Figure 4b, the change in the synaptic weight versus the relative spike timing can be fitted with exponential decay functions:[41]

$$\Delta w = \begin{cases} A_+ e^{-|\Delta t|/\tau_+}, & \Delta t > 0 \\ A_- e^{-|\Delta t|/\tau_-}, & \Delta t < 0 \end{cases} \quad (1)$$

where Δw is the percentage change of the synaptic weight with respect to the lowest conductance in the positive part and the highest conductance in the negative part, Δt the relative spiking timing, and A_+/A_- the scaling factor, whereas τ_+/τ_- the time constant for the positive and negative Δt, respectively. The values for A_+/A_- are 134.8/−163.7, and the ones for τ_+/τ_- are 68.6/−226.4 μs, confirming that the STDP characteristics similar to that of biological synaptic systems can indeed be mimicked using this memristive device. During the STDP measurement, the synaptic weight was recorded only after paired spikes (i.e., simultaneous presynaptic and postsynaptic spikes) had been applied to the device for 2000 s. This is to ensure the stability of the conductance at the time of recording as well as to follow the standard practice in biology of taking STDP data 30–40 min after applying the spike.[41,42] In fact, the instinctive decay of EPSC after stimulation makes the behavior of STDP highly dependent on the amount of time elapsed since the application of paired spikes, as evidenced by the results in Figure S1 (Supporting Information) where the conductance is measured at 1, 10, 100, 1000, and 2000 s after applying the paired spikes.

The effect of metaplasticity on STDP was firstly studied by changing the synaptic plasticity of the WO_3 memristive device using different spike history. In this regard, a more stable, easily controllable, and relatively small range of plasticity modulation was used,[6,8–10,13–15,20] with the I–V curves and good retention shown in Figure S2 (Supporting Information). The effect of metaplasticity on STDP is demonstrated in **Figure 5**. First of all, five cycles of consecutive conductance change were realized and shown in Figure 5a, with the third cycle of the conductance change and the applied pulses given in Figure 5b for clarity. Then, the effect of metaplasticity on STDP was tested using three different kinds of paired spike sequence, marked as Seq. 1, Seq. 2, and Seq. 3, respectively. Figure 5c shows the STDP due to Seq. 1 with marked spike number. During the first ten potentiation spikes, which potentiates the plasticity of the memristive device, the relative timing between pre- and postsynaptic actions decreases one by one and the synaptic weight increases accordingly. During the next ten depression spikes, the relative timing decreases gradually and the corresponding synaptic weight changes coincidently. Whether due to potentiation or depression spikes, the least timing between pre- and postsynaptic actions generates the strongest change of the synaptic plasticity, just as the Hebbian learning rule suggests.[2] The STDP due to Seq. 2 and 3 are shown in Figure 5d and Figure 5e, respectively. For a clear comparison, these three STDP curves are compiled in Figure 5f with the precisely designed pre- and postsynaptic spikes plotted in the inset. It becomes obvious that the STDP behaviors of the WO_3 memristive device undergoing different stimulus history are quite different, which should be due to the change of plasticity by the previous stimulus. For example, although the spike sequence in the positive part of STDP in Figure 5d is the same as that in

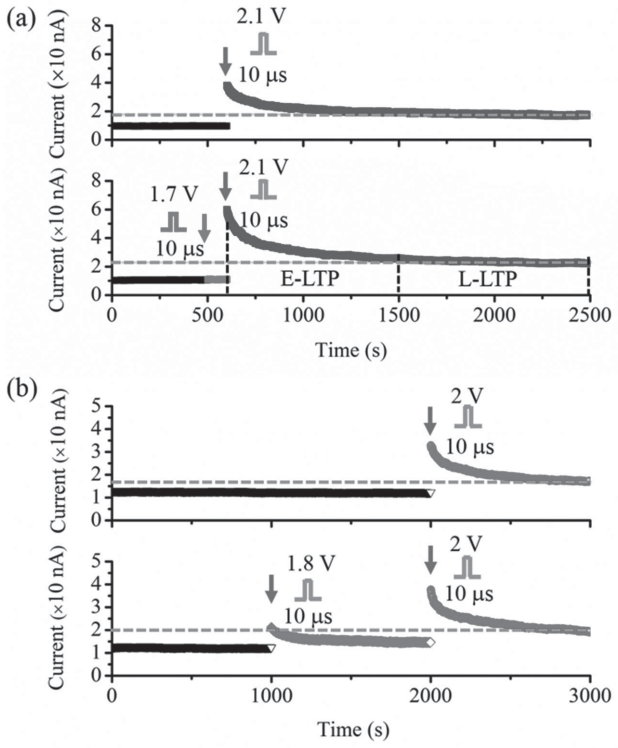

Figure 3. Excitatory postsynaptic current (EPSC). a) Typical metaplasticity with simple presynaptic spike. When applying a presynaptic spike (2.1 V, 10 μs), EPSC is triggered and measured in the upper panel. With negative voltage pulse, such device goes back to the original state and is relaxed for one day. Subsequently, with a priming spike (1.7 V, 10 μs), no obvious current change is observed. Then another presynaptic spike (2.1 V, 10 μs) is applied and the generated EPSC is recorded in the lower panel. The former part of EPSC corresponds to early-form LTP (E-LTP) and the latter to the late LTP (L-LTP). b) Another case of metaplasticity. EPSC is triggered immediately with a presynaptic spike (2 V, 10 μs) in the upper panel. For comparison, after recovering to the original state, a presynaptic spike (1.8 V, 10 μs) is applied and triggers EPSC. Afterward another presynaptic spike (2 V, 10 μs) is applied and triggers a larger EPSC, measured in the lower panel. All the current is read at 0.05 V.

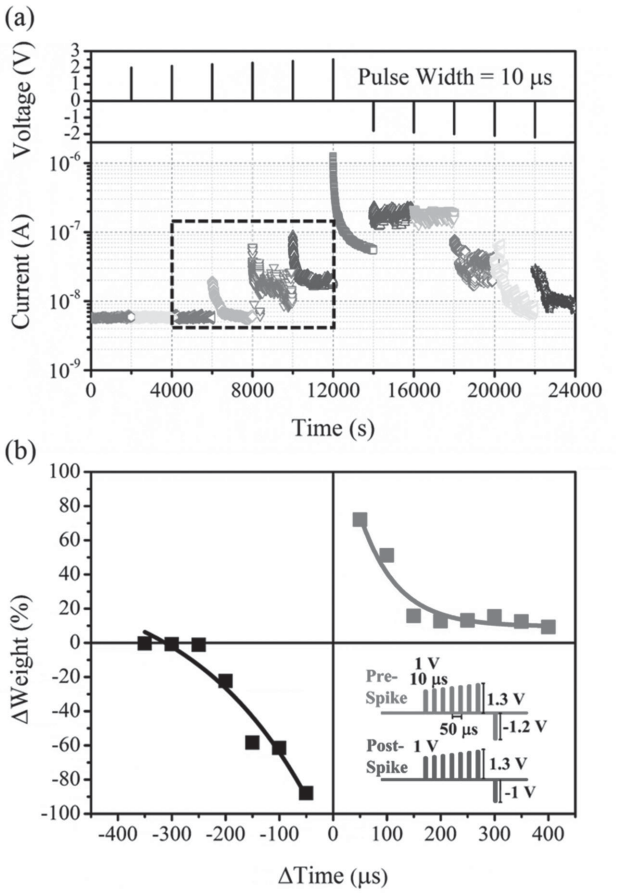

Figure 4. Demonstration of STDP in Pt/WO_3/Pt memristive device. a) Current decay following the application of a sequence of positive and negative pulses with read voltage of 0.05 V. The volatile to nonvolatile transition is indicated in the dotted square. b) Change of the synaptic weight (taken after the application of the paired spikes for 2000 s) versus the relative timing of the artificial neuron with pre-spike and post-spike in the inset.

Figure 5e, the different spike sequences in the negative part still cause quite different behaviors of STDP in the positive part. The spikes in the negative part change the plasticity or the ability to alter the plasticity. In turn, this different activity sequences results in different STDPs in the negative part. Such a phenomenon should be taken into consideration while developing neuromorphic computing based on synapse emulating devices.

Due to the time-decaying property of EPSC as shown in Figures 3 and 4b, the interval between presynaptic spikes is another very important issue for the development of neuromorphic computing. Some studies on the effect of spike interval on the synaptic plasticity discovered a transition from the short-term plasticity to the long-term plasticity[24] as well as the phenomenon of paired-pulse facilitation (PPF).[43,44] Ohno et al. reported that in the Ag_2S inorganic synapse, the devices stored information as short-term plasticity with a spontaneous decay of conductance in response to intermittent input stimuli, whereas the frequent stimulation resulted in a transition to the long-term plasticity.[24] According to a study by Zhu et al. on oxide-based artificial synapse laterally coupled by proton neurotransmitters, the peak value of the EPSC triggered by the second presynaptic spike is higher than that by the first, and the amplitude ratio between the second and the first EPSCs, defined as the "PPF index," is a function of the spike interval.[43] Therefore, the interval between the pre-spike and next spike determines the state of the artificial synapse in some sense; the interval should also affect the behaviors of STDP although further supports are needed.

The effect of spike interval as another metaplasticity effect on STDP was also studied and the results are shown in **Figure 6**. Starting with the same original state, a series of paired spikes were applied to the device at intervals of 500, 100, 10, and 1 s, respectively, the triggered EPSC was recorded as the synaptic weight, and the corresponding STDP was obtained from the synaptic weight one interval after the application of the paired spikes. The obtained STDPs are compiled together for different spike intervals in Figure 6h, and the differences show up. All of the STDP curves are fitted by Equation (1) and the related time constant are also given in Figure 6. One can see that the spike

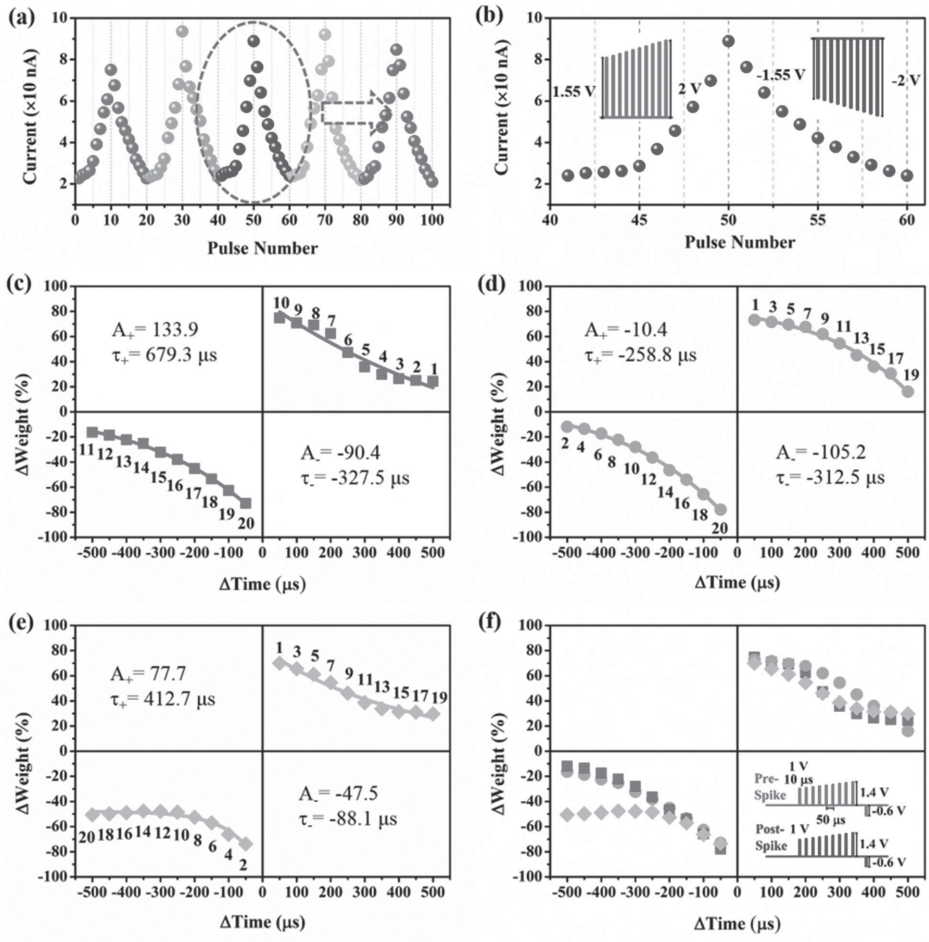

Figure 5. Effect of activity sequences on STDP. a) Conductance change cycles by consecutive potentiating or depressing pulses. b) One of the above cycles with the pulses in the inset. STDP resulted from three typical stimulating sequences are shown in panels (c)–(e), respectively, which are compiled in panel (f) with the pre-spike and post-spike in the inset.

interval indeed matters a lot to the STDP based on the memristive device, and should be seriously taken into account when designing neuromorphic computing. Perhaps, one can take full advantage of it, so that a time-related neuromorphic computing, similarly to the brain, can be attainable. In fact, by modifying the time parameter, different time constants for STDP curves can be obtained in one simple memristive device. In biological synaptic plasticity studies, such STDP behavior is related to the Ca^{2+} dynamics.[45] When modeling STDP, adjusting one of the Ca^{2+}-related dynamic parameters can result in different STDP behaviors with different time constants.[45] In this work, Seq. 1 was used as the paired spike sequence for the EPSC and STDP results in Figure 6. For the other two paired spike sequences, the triggered EPSC and the corresponding spike interval effect on STDP are given in Figures S3 and S4 (Supporting Information). Furthermore, the activity sequence effect of the metaplasticity on STDP with different intervals of paired spikes is compared in Figure S5 (supporting information), which is similarly discussed in Figure 5. Thus, for the study of STDP in synapse-emulating memristive devices, we suggest specific documentation of the sequence and the interval of paired spikes as well as the time to record STDP since applying the spike. Recently, it was reported that using non-overlapping spiking pulse protocol, instead of the traditional overlapping one,[7–15] in second-order memristors, should be more bio-realistic to emulate the internal cause that leads to the apparent learning rule, and should facilitate the development of complete theoretical and experimental frameworks for neuromorphic computing system.[21,46] We believe that the as-discussed metaplasticity effect on STDP should also be considered, which does not necessarily depend on the spiking pulse protocol being used.

The resistive switching mechanism in WO_3 thin films was widely discussed in previous studies;[26,34,35] in most cases, the migration of oxygen ions (or oxygen vacancies, V_O) is suggested to play a key role. In this work, the observed conductive Magnéli phase clearly supports the assumption that oxygen vacancies are created in the vicinity of the anode according to the electrochemical reaction, $O_O^{\times} \leftrightarrow V_O + 2e' + 1/2O_2(\uparrow)$, and migrate to the cathode under the applied electric field, resulting in the vacancy accumulation at the cathode, and giving rise to the growth of an oxygen-vacancy-enriched phase starting from the cathode and heading for the anode during electroforming (Figure 2f).[34,37] It should be pointed out that the conductive Magnéli phase does not span the entire WO_3 film thickness

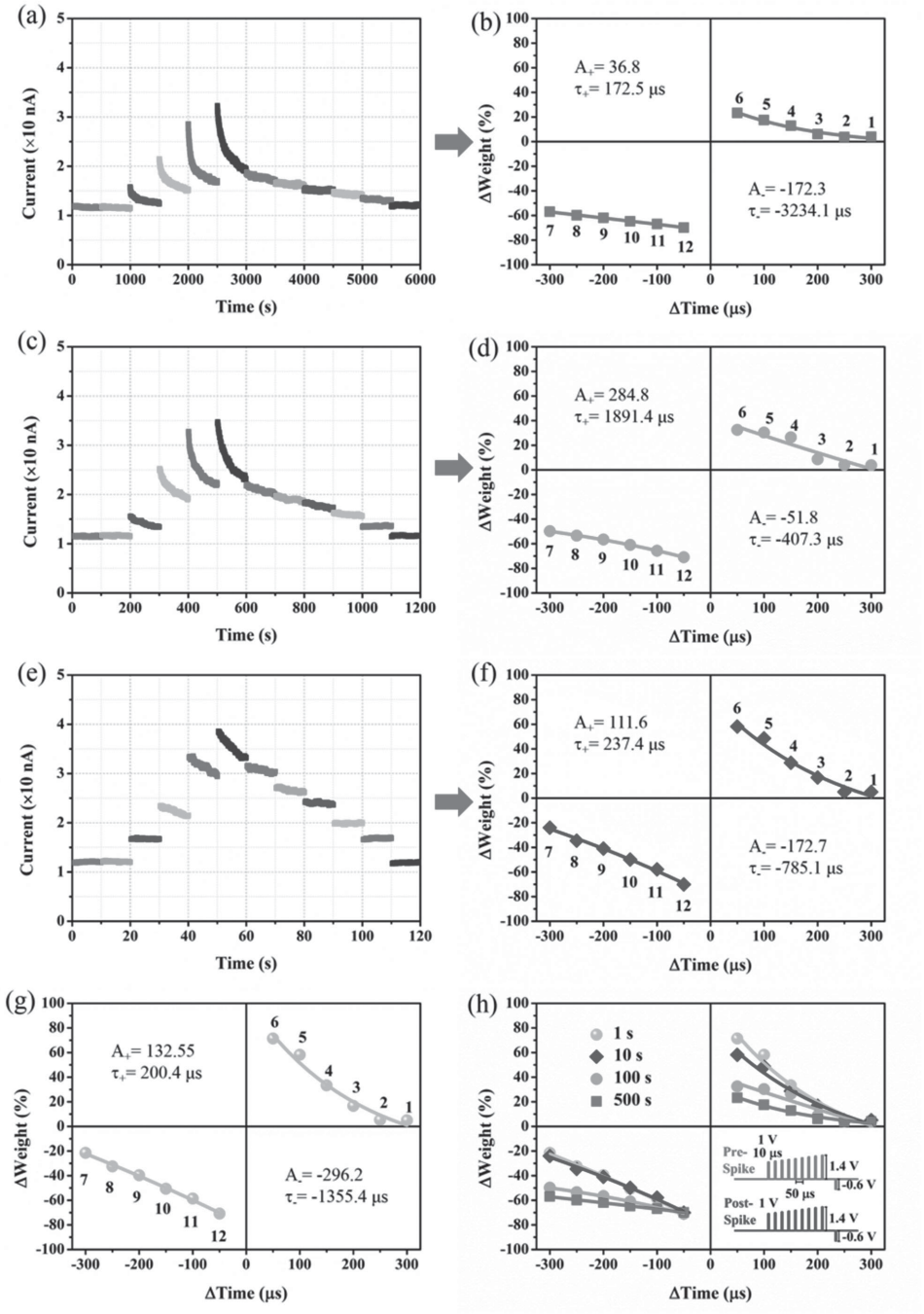

Figure 6. Effect of spike interval on STDP. Measured synaptic weight with an interval of a) 500 s, c) 100 s, e) 10 s for each paired spike and resulted STDP with the marked spike sequence in panels (b), (d), and (f), respectively. g) STDP taken after an interval of 1 s for each paired spikes. h) Comparison of STDP behaviors with different intervals. Inset: prespike and postspike. All the current is read at 0.05 V.

and a gap is formed between the cathode and the tip of the conductive phase, as demonstrated in Figure 2f. With this observation and the common understanding of the resistive switching in WO_3-based memristors,[26,46] it is believed that the migration of oxygen vacancies and the resultant modulation of the gap should be responsible for the resistive switching and the current decay. The diffusion coefficient of oxygen vacancies is estimated to be $\approx 2.4 \times 10^{-17}$ m^2 s^{-1} with the Cottrell equation reported by Messerschmitt et al.[47] and Nili et al.[48] (see Figure S6 and related text in the Supporting Information). Compared with those reported in previous works,[49–51] the diffusion coefficient is high, which might be due to the overestimated diffusion distance, which is taken as the film thickness for simplicity. However, vacancies only have to move over the distance between the conductive Magnéli phase and the counter electrode,[37,52] which is a small fraction of the film thickness.

The vacancy migration can be driven both by the electric field and the spontaneous diffusion.[46] Upon applying an electrical stimulus, oxygen vacancies should be activated to migrate more easily with the subsequent spikes as in the case for Figure 3. The state of activated oxygen vacancies determines the ability to generate the synaptic plasticity, which could be the cause of the metaplasticity in our memristive devices. The EPSC decay is due to the relaxation of activated oxygen vacancies at some extent before reaching another state, implying the existence of other internal states to allow mimicking STDP by taking the non-overlapping spiking pulse protocol as a second-order memristor. However, the specific mechanism of metaplasticity, together with internal states in these memristive devices, needs further detailed research in the future.

In summary, we present a simple WO_3-based memristive device as an artificial synapse exhibiting neuromorphic functions, and a connection is firstly established between the biological term of metaplasticity and the activity-dependent plasticity of the artificial synapse. The effects of metaplasticity on the neuromorphic function based on STDP are systematically discussed in terms of activity sequence and stimulus interval. The significance of metaplasticity lies in that the stimulus history has an important influence on the device state at the moment when a following stimulus is executed, thus affects the eventual neuromorphic functions. Although the effect of the metaplasticity is only discussed for STDP in the WO_3 device here, the synaptic plasticity related neural functions exhibited in many other memristive devices should also be carefully dealt with, as the current or conductance-decaying phenomenon is widely observed in memristive devices. This work provides guidance for future neuromorphic computing systems using memristive devices.

Experimental Section

Sample Preparation: The simple oxide memristive device consisted of ≈80 nm thick Pt films as bottom and top electrodes and ≈150 nm thick WO_3 thin film as resistive-switching layer. It was fabricated on a quartz substrate and exhibited a crossbar structure with a junction area of 50 × 50 μm as shown in Figure 2a. Both Pt electrodes were deposited in an Ar environment through a metal mask. The WO_3 thin film was prepared by radio frequency sputtering in a gas mixture containing 80% Ar and 20% O_2 at a pressure of 0.93 Pa, followed by in situ annealing at 300 °C in an oxidizing atmosphere containing 50% Ar and 50% O_2 at a pressure of 2.67 Pa.

Device Electrical Measurement: All the measurements were performed with a Keithley 4200 Semiconductor Characterization System connected with a Cascade SUMMIT 11000B semi-automatic probe station in air and at the room temperature.

Supporting Information

Supporting Information is available from the Wiley Online Library or from the author.

Acknowledgements

Z.-H.T. and R.Y. contributed equally to this work. This work was supported by the National Natural Science Foundation of China (Grant Nos. 51372094 and 51302095), the Opening Project of State Key Laboratory of High Performance Ceramics and Superfine Microstructure (SKL201408SIC), and Fundamental Research Funds for the Central Universities (2014TS024).

Received: July 23, 2015
Revised: September 17, 2015
Published online: November 17, 2015

[1] M. M. Waldrop, *Nature* **2013**, *503*, 22.
[2] D. O. Hebb, *The Organization of Behavior: A Neurophysiological Theory*, Wiley, New York **1949**.
[3] W. C. Abraham, *Nat. Rev. Neurosci.* **2008**, *9*, 387.
[4] W. C. Abraham, M. F. Bear, *Trends Neurosci.* **1996**, *19*, 126.
[5] W. C. Abraham, W. P. Tate, *Prog. Neurobiol.* **1997**, *52*, 303.
[6] S. H. Jo, T. Chang, I. Ebong, B. B. Bhadviya, P. Mazumder, W. D. Lu, *Nano Lett.* **2010**, *10*, 1297.
[7] D. Kuzum, R. G. D. Jeyasingh, B. Lee, H. S. P. Wong, *Nano Lett.* **2012**, *12*, 2179.
[8] F. Alibart, S. Pleutin, O. Bichler, C. Gamrat, T. Serrano-Gotarredona, B. Linares-Barranco, D. Vuillaume, *Adv. Funct. Mater.* **2012**, *22*, 609.
[9] Z. Q. Wang, H. Y. Xu, X. H. Li, H. Yu, Y. C. Liu, X. J. Zhu, *Adv. Funct. Mater.* **2012**, *22*, 2759.
[10] P. Krzysteczko, J. Munchenberger, M. Schafers, G. Reiss, A. Thomas, *Adv. Mater.* **2012**, *24*, 762.
[11] Y. Li, Y. P. Zhong, L. Xu, J. J. Zhang, X. H. Xu, H. J. Sun, X. S. Miao, *Sci. Rep.* **2013**, *3*, 1619.
[12] A. Williamson, L. Schumann, L. Hiller, F. Klefenz, I. Hoerselmann, P. Husar, A. Schober, *Nanoscale* **2013**, *5*, 7297.
[13] Y. Li, Y. P. Zhong, J. J. Zhang, L. Xu, Q. Wang, H. J. Sun, H. Tong, X. M. Cheng, X. S. Miao, *Sci. Rep.* **2014**, *4*, 4906.
[14] S. Kim, S. Choi, J. Lee, W. D. Lu, *ACS Nano* **2014**, *8*, 10262.
[15] W. He, K. J. Huang, N. Ning, K. Ramanathan, G. Q. Li, Y. Jiang, J. Sze, L. P. Shi, R. Zhao, J. Pei, *Sci. Rep.* **2014**, *4*, 4755.
[16] M. Suri, O. Bichler, Q. Hubert, L. Perniola, V. Sousa, C. Jahan, D. Vuillaume, C. Gamrat, B. DeSalvo, *Solid State Electron.* **2013**, *79*, 227.
[17] K. V. Egorov, R. V. Kirtaev, Y. Y. Lebedinskii, A. M. Markeev, Y. A. Matveyev, O. M. Orlov, A. V. Zablotskiy, A. V. Zenkevich, *Phys. Status Solidi A* **2015**, *212*, 809.
[18] D. Garbin, E. Vianello, O. Bichler, Q. Rafhay, C. Gamrat, G. Ghibaudo, B. DeSalvo, L. Perniola, *IEEE Trans. Electron Devices* **2015**, *62*, 2494.
[19] Y. Matveyev, K. Egorov, A. Markeev, A. Zenkevich, *J. Appl. Phys.* **2015**, *117*, 044901.
[20] S. Mandal, A. El-Amin, K. Alexander, B. Rajendran, R. Jha, *Sci. Rep.* **2014**, *4*, 5333.
[21] S. Kim, C. Du, P. Sheridan, W. Ma, S. Choi, W. D. Lu, *Nano Lett.* **2015**, *15*, 9.
[22] E. Fino, V. Paille, J. M. Deniau, L. Venance, *Neuroscience* **2009**, *160*, 744.
[23] M. Fuenzalida, D. Fernandez de Sevilla, W. Buno, *J. Neurosci.* **2007**, *27*, 11940.
[24] T. Ohno, T. Hasegawa, T. Tsuruoka, K. Terabe, J. K. Gimzewski, M. Aono, *Nat. Mater.* **2011**, *10*, 591.
[25] S. La Barbera, D. Vuillaume, F. Alibart, *ACS Nano* **2015**, *9*, 941.
[26] T. Chang, S. H. Jo, W. D. Lu, *ACS Nano* **2011**, *5*, 7669.
[27] E. Mikheev, B. D. Hoskins, D. B. Strukov, S. Stemmer, *Nat. Commun.* **2014**, *5*, 3990.
[28] D. S. Jeong, R. Thomas, R. S. Katiyar, J. F. Scott, H. Kohlstedt, A. Petraru, C. S. Hwang, *Rep. Prog. Phys.* **2012**, *75*, 076502.
[29] J. Y. Raty, W. Zhang, J. Luckas, C. Chen, R. Mazzarello, C. Bichara, M. Wuttig, *Nat. Commun.* **2015**, *6*, 7467.

[30] J. L. M. Oosthoek, D. Krebs, M. Salinga, D. J. Gravesteijn, G. A. M. Hurkx, B. J. Kooi, *J. Appl. Phys.* **2012**, *112*, 084506.
[31] D. Ielmini, A. L. Lacaita, D. Mantegazza, *IEEE Trans. Electron Devices* **2007**, *54*, 308.
[32] M. Boniardi, D. Ielmini, *Appl. Phys. Lett.* **2011**, *98*, 243506.
[33] F. Messerschmitt, M. Kubicek, J. L. M. Rupp, *Adv. Funct. Mater.* **2015**, *25*, 9.
[34] R. Yang, K. Terabe, T. Tsuruoka, T. Hasegawa, M. Aono, *Appl. Phys. Lett.* **2012**, *100*, 231603.
[35] R. Yang, K. Terabe, G. Q. Liu, T. Tsuruoka, T. Hasegawa, J. K. Gimzewski, M. Aono, *ACS Nano* **2012**, *6*, 9515.
[36] K. Szot, W. Speier, G. Bihlmayer, R. Waser, *Nat. Mater.* **2006**, *5*, 312.
[37] K. J. Yoon, S. J. Song, J. Y. Seok, J. H. Yoon, T. H. Park, D. E. Kwon, C. S. Hwang, *Nanoscale* **2014**, *6*, 2161.
[38] J. D. Sweatt, *Learn. Mem.* **1999**, *6*, 399.
[39] J. L. McGaugh, *Science* **2000**, *287*, 248.
[40] R. M. Shiffrin, R. C. Atkinson, *Psychol. Rev.* **1969**, *76*, 15.
[41] R. C. Froemke, Y. Dan, *Nature* **2002**, *416*, 433.
[42] M. Nishiyama, K. Hong, K. Mikoshiba, M. Poo, K. Kato, *Nature* **2000**, *408*, 584.
[43] L. Q. Zhu, C. J. Wan, L. Q. Guo, Y. Shi, Q. Wan, *Nat. Commun.* **2014**, *5*, 3158.
[44] R. Yang, K. Terabe, Y. P. Yao, T. Tsuruoka, T. Hasegawa, J. K. Gimzewski, M. Aono, *Nanotechnology* **2013**, *24*, 384003.
[45] H. Z. Shouval, M. F. Bear, L. N. Cooper, *Proc. Natl. Acad. Sci. USA* **2002**, *99*, 10831.
[46] C. Du, W. Ma, T. Chang, P. Sheridan, W. D. Lu, *Adv. Funct. Mater.* **2015**, *25*, 4290.
[47] F. Messerschmitt, M. Kubicek, S. Schweiger, J. L. M. Rupp, *Adv. Funct. Mater.* **2014**, *24*, 7448.
[48] H. Nili, S. Walia, A. E. Kandjani, R. Ramanathan, P. Gutruf, T. Ahmed, S. Balendhran, V. Bansal, D. B. Strukov, O. Kavehei, M. Bhaskaran, S. Sriram, *Adv. Funct. Mater.* **2015**, *25*, 3172.
[49] M. Metikos-Hukovic, Z. Grubac, *J. Electroanal. Chem.* **2003**, *556*, 167.
[50] E. Sikora, J. Sikora, D. Macdonald, *Electrochim. Acta* **1996**, *41*, 7.
[51] M. Bojinov, *Electrochim. Acta* **1997**, *42*, 10.
[52] D. S. Hong, Y. S. Chen, Y. Li, H. W. Yang, L. L. Wei, B. G. Shen, J. R. Sun, *Sci. Rep.* **2014**, *4*, 4058.